THE ASTROPHYSICAL JOURNAL, 383:226–232, 1991 December 10

EVIDENCE FOR A THERMALLY UNSTABLE SHOCK WAVE IN THE VELA SUPERNOVA REMNANT

JOHN C. RAYMOND[1]
Harvard-Smithsonian Center for Astrophysics, 60 Garden Street, Cambridge, MA 02138

AND

GEORGE WALLERSTEIN[1] AND BRUCE BALICK[1]
Department of Astronomy FM-20, University of Washington, Seattle, WA 98195
Received 1991 April 29; accepted 1991 June 17

ABSTRACT

The emission- and absorption-line signatures of supernova remnant shock waves provide complementary diagnostic capabilities. This paper presents *IUE* spectra of the nebulosity and new spectra of HD 72088. We use models of the emission and absorption lines from shocked gas to derive a shock velocity and elemental depletions. There is evidence from the absorption-line strengths and widths for thermally unstable cooling behind a 150 km s^{-1} shock. We confirm the shock velocity and swept-up column density estimates of Wallerstein & Balick, and we find evidence for a nonthermal contribution to the pressure.

Subject headings: nebulae: individual (Vela Supernova Remnant) — nebulae: supernova remnants — shock waves — stars: individual (HD 72088)

1. INTRODUCTION

Supernova remnant shock waves strongly affect the density and temperature structure of the interstellar medium, and they allow us to probe the conditions in the vicinity of the supernova. The combination of UV emission-line intensities with optical spectra and images provides enormous leverage. With sufficient observables, we can test shock models and fix the essential shock parameters; velocity, preshock density and ionization state, elemental abundances, and column density of swept-up gas (Benvenuti, Dopita, & D'Odorico 1980; Raymond et al. 1980, 1981; Raymond et al. 1988, hereafter RHCBFG).

Studies of absorption lines in the spectra of stars behind supernova remnants provide a nearly orthogonal set of information. They are sensitive to cooler, lower density gas, and to ions whose emission lines are weak or blended with stronger lines at *IUE* resolution (Jenkins, Silk, & Wallerstein 1976; Jenkins, Wallerstein, & Silk 1984, hereafter JWS; Fesen et al. 1988). Just as combining optical and UV emission spectra greatly increases the power of the data to test shock models and determine model parameters, joining emission and absorption studies can reveal properties of the shocked gas not derivable from either data set alone.

Such a combination of emission- and absorption-line studies requires a fortunate coincidence between a hot, bright background star and a patch of nebulosity bright enough for emission-line work. Wallerstein & Balick (1990, hereafter WB) have surveyed the neighborhoods of the stars behind the Vela supernova remnant observed by JWS, and they found fairly bright nebulosity around two stars. We have selected the B3 III star HD 72088 for further study. Its absorption spectrum shows a +94 km s^{-1} component in high ionization species (JWS), and CTIO long-slit spectra show strong emission close to the star (WB). We have obtained *IUE* spectra of the nebulosity close to the star and some additional high-dispersion spectra of the star itself. We compare these observations with models of incomplete radiative shocks to derive shock parameters and elemental depletions. The absorption lines require a shock velocity of 150 km s^{-1}, a swept-up column density of about 10^{18} cm^{-2}, and very little depletion of carbon. The emission lines of the bright nebulosity 45″ from the star require a smaller shock velocity and a somewhat larger swept-up column. We find tentative evidence for thermally unstable cooling of the shocked gas as predicted by Chevalier & Imamura (1982) and Innes, Giddings, & Falle (1987). There is some evidence for depletion of carbon and silicon, and some evidence that the shock ram pressure greatly exceeds the thermal pressure in the postshock region.

2. OBSERVATIONS

We observed HD 72088 and the nebulosity near it with the *IUE* satellite in 1990 May and October. Boggess et al. (1978) describe the *IUE* instrument. Table 1 lists the spectra with the offsets from HD 72088, exposure times, and position angles of the 10″ by 20″ large aperture (east of north). The *IUE* aperture for SWP 39996 and LWP 19086 was just beyond the western edge of the [O III] and Hα images of WB to the east of the star. Spectra were extracted from the line-by-line files of the Guest Observer tapes after removal of cosmic rays and hot pixels. Three sections across the large aperture were extracted, but the individual spectra are noisy, and no remarkable changes in relative line intensities across the aperture are apparent. Therefore, we present only the total spectrum for each exposure. Figure 1 shows the spectra extracted from SWP 39996 and LWP 19086.

The first two nebular exposures were placed as close as possible to the star. A large aperture shutter operation a day or so earlier caused a 2″ pointing glitch during the SWP 38713 exposure. This glitch moved the aperture closer to the star, and the exposure is so heavily contaminated with scattered stellar continuum that much of the spectrum is overexposed. The second exposure, SWP 38718, is somewhat contaminated by stellar

[1] Guest Observer with the *International Ultraviolet Explorer* satellite, which is jointly operated by NASA, the Science Research Council of the UK, and the European Space Agency.

TABLE 1

IUE IMAGES

Image	Dispersion	Offset	Position Angle	Exposure (minutes)
SWP 38713	Low	13″N, 5″W	−6°	440
SWP 38718	Low	0 N, 12 E	−5	620
SWP 39986	Low	0 N, 35 E	−191	400
SWP 39996	Low	0 N, 45 E	−190	360
SWP 39997	Low	64 N, 60 E	−190	220
LWP 19806	Low	0 N, 45 E	−190	290
SWP 38714	High	...	...	140
SWP 38715	High	...	...	87
LWP 17846	High	...	...	70
LWP 18847	High	...	...	75

continuum, and the line emission is very faint. The C III] intensity is 0.85×10^{-13} ergs cm^{-2} s^{-1}, Si III] λ1896 is 0.8 times as bright. A sky background exposure, SWP 39997, was obtained simultaneously with LWP 19806 at a position fixed by the spacecraft roll angle and the distance between the apertures. It does not lie on any [O III] nebulosity or on any bright Hα filamentary structure, but the entire region shows diffuse Hα emission from the Gum nebula. No emission lines are detected, but an apparent continuum which could be background two-photon continuum or a camera artifact (see Crenshaw, Breugman, & Norman 1990) is present.

Table 2 presents the line and continuum fluxes measured from the three remaining exposures. The uncertainties are about 10% for the strongest lines and about 30% for the weaker lines, due to uncertainty in baseline placement and to hot pixels located near the O III] and N III] lines. Two values for each of the SWP continuum fluxes are given. The higher is the value measured directly, while the lower is the value obtained after the sky background spectrum (SWP 39997 smoothed over 50 points) is subtracted. We believe that the latter number is more realistic, but the uncertainty is large.

To supplement the spectra of the emission filaments, we have also analyzed high-resolution spectra of HD 72088. In the short wavelength region we stacked two archival spectra obtained by JWS (SWP 5552 and SWP 10497) with the two new ones, and in the long wavelength range we combined two new spectra for analysis. Figure 2 shows the profiles of the C IV

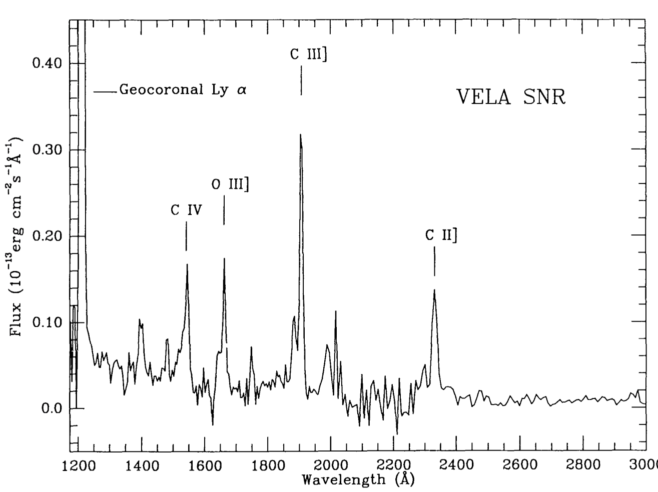

FIG. 1.—*IUE* low-dispersion spectra of the nebulosity 45″ east of HD 72088.

TABLE 2

MEASURED LINE AND CONTINUUM FLUXES[a]

Ion	Wavelength	SWP 39986	SWP 39996	LWP 19086
N V	1240	≤0.2	≤0.25	...
O IV], Si IV	1400	0.48	1.0	...
N IV]	1486	≤0.3	0.47	...
C IV	1550	1.0	1.7	...
O III]	1664	1.1	1.8	...
N III]	1750	0.1	0.4	...
Si III]	1890	1.2	1.4	...
C III]	1909	3.7	3.7	...
C II]	2325	...	...	2.3
[Ne IV]	2425	...	...	≤0.4
Continuum	1300	0.02–0.055	0.02–0.054	...
	1800	0.01–0.024	0.01–0.027	...
	2700	...	...	0.0074

[a] Units: 10^{-13} ergs cm^{-2} s^{-1} or 10^{-13} ergs cm^{-2} s^{-1} Å^{-1}.

and Mg II doublets. Except for C I, we analyze only the +80 to +135 km s^{-1} (LSR) feature, because the low-velocity absorption arises in foreground or even background material, since the distance to HD 72088 is about 2.0 kpc. For C I the low-velocity lines are rather weak and lines arising from the excited fine structure levels were also measured to get an indication of preshock conditions. Supernova remnant absorption may be present on the blue sides of the low-velocity absorption lines as well as on the red sides, but stellar absorption features are clearly present (strong lines arising from excited levels which are not populated at the interstellar densities are detected), and they show blue wings presumably arising in a wind. Thus we have no absorption line information about the approaching shock wave on the near side of the Vela SNR.

In Table 3 we show the resulting equivalent widths and column densities for the high-velocity component and for the low velocity C I, C I*, and C I** lines. The lines are not very strong, so curve-of-growth analysis yields fairly good column density data but does not establish the velocity parameter "b" except to indicate that 5 km s^{-1} is too small. Hence we use $b = 15$ km s^{-1} for the high-velocity components to represent the range of 10–20 km s^{-1} which is allowed by the C IV and Mg II doublets.

For C I a b-value of 5 km s^{-1} could be excluded and 8 km s^{-1} is unlikely, so we used $b = 10$ km s^{-1} to derive column densities for C I, C I*, and C I** of 14.4, 13.8, and 13.4, respectively. Thus C I*/C $\text{I}_{\text{total}} = 0.19$ and C I**/C $\text{I}_{\text{total}} = 0.07$. By following the analysis of Jenkins & Shaya (1979) Figure 6*b*,

TABLE 3

EQUIVALENT WIDTHS AND COLUMN DENSITIES OF HIGH-VELOCITY GAS DERIVED FROM ABSORPTION LINES IN HD 72088

Ion	Line (Å)	$-\log(W/\lambda)$	$\log(N)$ (cm^{-2})	6 μG	12 μG
C II*	1335.71	4.31	13.3	14.03	13.68
C IV	1548.20	4.12	13.7	13.45	13.48
	1550.77	4.34	13.6	13.45	13.48
N V	1238.82	≤4.62	≤13.2	12.57	12.33
Mg II	2795.53	4.35	12.55	12.58	12.51
	2802.70	4.52	12.65	12.58	12.51
Si II	1260.42	3.83	13.1	13.23	13.20
	1526.71	4.13	13.8	13.23	13.20
Si IV	1402.77[a]	≤4.55	≤13.0	12.98	13.00
Fe II	2599.40[b]	≤4.60	≤12.8	13.05	12.75

[a] The line at 1393.71 Å is noiser and less useful.

[b] The line at 2585.88 Å is also absent but has a smaller *f*-value.

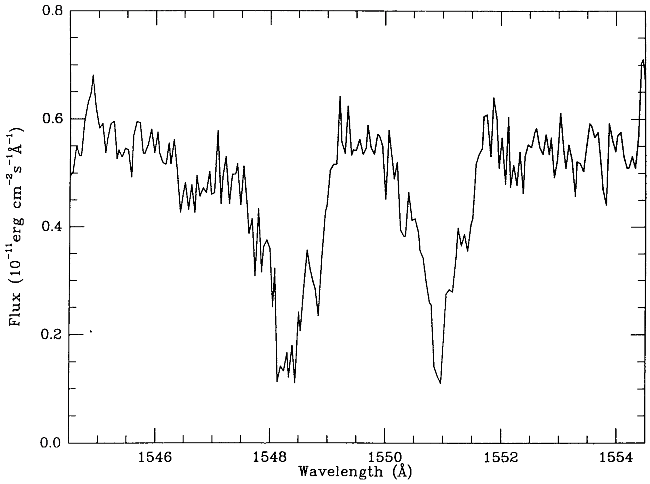

FIG. 2a

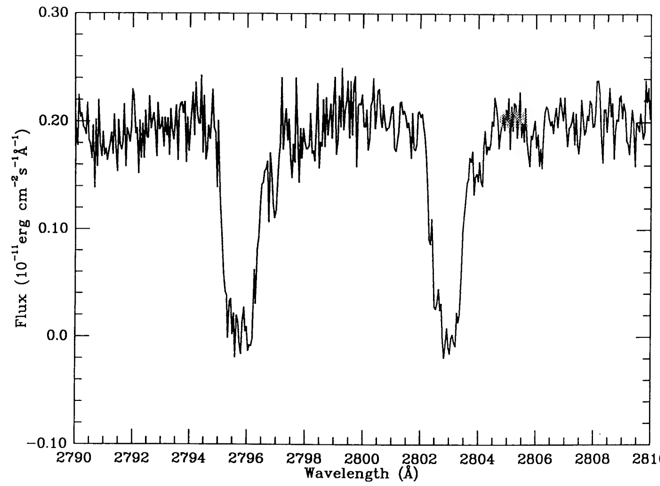

FIG. 2b

FIG. 2.—(a) C IV absorption profiles from average of four spectra of HD 72088. (b) Mg II absorption profiles from average of two spectra of HD 72088.

which is computed for an interstellar radiation field 10 times the field in the solar vicinity, we find little sensitivity to the kinetic temperature and log $(p/k) = \log(nT) \leq 3$. Thus for $T = 100$ K, $n \leq 10$ cm^{-3}. This is reasonable in light of the upper limit of 70 cm^{-3} derived from the [S II] doublet in emission (WB) and the density estimate from the C III] surface brightness derived below, both of which refer to the shocked gas.

All of the high-velocity absorption features seen in Figure 2 are wider than the *IUE* spectral resolution of about 25 km s^{-1}. After correcting for the *IUE* spectral response, the absorption lines extend over the range +85 to +135 km s^{-1} (LSR). The depths of the high-velocity features are around 50% of the continuum level, so the lines are probably unsaturated. While it is conceivable that each absorption feature contains several unresolved features, the equivalent width of each narrow feature would be less than 50 mÅ, so the lines almost certainly lie on the linear part of the curve of growth. The Si II λ1260 line is a possible exception, being nearly twice as strong as the other lines, but even that cannot be very highly saturated. Caution must be used in interpreting *IUE* line profiles, but we are convinced that the widths of the lines are real. They are seen in all the individual exposures, so their width is not an artifact of adding improperly registered spectra. All the observed features in the summed spectra, two doublet members each of C IV and Mg II, as well as the C II* and Si II lines, show essentially the same velocity width.

It is difficult to estimate the equivalent width uncertainty involved in separating the high-velocity component from the much stronger zero velocity component, but the consistency of the doublet ratios at line widths expected for shock-heated gas leads us to believe that the column densities are accurate to about 30%. Si II presents a problem, however, in that the lines at λ1260 and λ1526 yield different column densities. Sophisticated calculations consistently give a ratio of 10 between the oscillator strengths of these lines, but interstellar absorption line measurements generally suggest a smaller ratio (Luo, Pradhan, & Shull 1988). We adopt the average of the two column density determinations and take it to be uncertain by a factor of 2.

3. INTERPRETATION

3.1. *General Characteristics of Radiative Shock Waves*

This section summarizes some properties of radiative shocks which will be useful in interpreting the observations, and it describes the model calculations which the subsequent sections will compare with the emission and absorption observations. More detailed discussions are available in McKee & Hollenbach (1980), Cox (1972), Shull & McKee (1979), and Raymond (1979). The parameters of a steady flow, plane-parallel shock are the shock velocity, preshock density, ionization state and magnetic field, total swept-up column density, and the elemental abundances (gas phase and grain). A shock driven by a pressure P should have an equal ram pressure ρv_s^2, so that the fast shocks which produce X-rays and the slower shocks we observe here have velocities related by the square root of the density contrast (McKee & Cowie 1975).

A radiative shock wave is one which radiates away most of the thermal energy of the shocked gas. When gas enters a strong shock, it is compressed by a factor of 4 and heated to $T_s = 1.4 \times 10^5 \times (v_s/100 \text{ km s}^{-1})^2$ K. T_s determines the highest ionization stage the gas can reach, a velocity near 100 km s^{-1} being needed to make O III and about 140 km s^{-1} to make N V. As soon as the gas is heated, it begins to cool by electron impact excitation of atoms and ions and the subsequent emission of photons. As the gas cools, it is compressed. Conservation of mass requires that the product $nv = n_0 v_s$. In the frame of the shock, $v = v_s/4$ just behind the shock, and by the time the gas cools to 10^4 K and undergoes a further order of magnitude compression, its velocity is only 1 or 2 km s^{-1}. From our point of view, the immediate postshock velocity is $3/4 v_s$, and the velocity in the recombining gas where the low-ionization species occur is very nearly v_s.

The scaling of the shock structure with n_0 is important to our interpretation. As the cooling rate scales as $n_e n$ and the thermal energy content scales as n, the cooling time and cooling length, l, scale as $1/n_e$, or as $1/n_0$. Emission-line intensities scale as $n_e nl$, so they increase as n_0. Ion column densities, which are the quantities measured by the absorption lines, scale as nl, and are therefore independent of n_0. The scaling breaks down if forbidden lines are collisionally quenched but that does not occur for the lines observed here. It also breaks down if magnetic pressure or some other mechanism prevents the compression of the cooling gas. The C II* column density is an exception to the n_0 independence of column densities, because the population of the excited level increases with density. For the conditions encountered in this shock, $N(\text{C II*}) \propto n_0$.

Model calculations integrate downstream from the shock front, and the endpoint of the integration, generally specified as the total column density swept-up, affects some of the predictions. The standard steady-flow shock models for optical and UV emission (Cox 1972; Shull & McKee 1979; Raymond 1979; Dopita, Binnette, & Tuohy 1984) cut off the integration when the gas cools to about 10^3 K, because there is almost no optical or UV radiation emitted at lower temperatures. Such a shock is called "complete," and the cutoff column density is not a model parameter. However, some SNR filaments, including the one analyzed below, show ratios of [O II] $\lambda3727$ and [O III] $\lambda5007$ to Hβ far larger than predicted by the steady-flow models (e.g., Fesen et al. 1982). These can be understood as recently formed shocks where the cooling and recombination do not reach completion (Raymond et al. 1980), and a model with the column density cutoff as a free parameter can successfully match the relative intensities of 30 optical and UV emission lines (RHCBTG). The cutoff is also important for column density predictions. While an ion such as C IV is formed at high enough temperature to be generally insensitive to the value of the cutoff, low-ionization species continue to increase in total column density as long as the integration continues. Thus while the cutoff is an "extra parameter" for matching emission line intensities, it is necessary for any prediction of the C II*, Si II, Mg II, or Fe II absorption lines in the high-velocity cloud.

The elemental abundances in the shocked gas are important for both emission- and absorption-line predictions. The models presented here assume the cosmic abundance set of Allen (1973); H = 12.0, C = 8.52, N = 7.96, O = 8.82, Ne = 7.92, Mg = 7.52, Si = 7.60, S = 7.20, and Fe = 7.60. We expect that He, O, N, Ne, and S will be undepleted, but that C, Mg, Si, and Fe are likely to be depleted onto refractory grains, and that they will be gradually returned to the gas phase by sputtering and by grain-grain collisions (Draine & Salpeter 1979; Seab & Shull 1983). Rather than attempt models with the additional free parameters of grain composition and size distribution and the imprecisely known rates of grain destruction, we compute models with the undepleted abundances and search for signatures of grain depletion in any differences between the models and observations.

An additional parameter which is not usually included in interstellar shock models is the ambient radiation field associated with the Gum nebula. This radiation can ionize the preshock gas and enhance the radiation from the recombination zone. In general, irradiation of the recombination zone will increase the Balmer line intensities and the strengths of the forbidden lines of singly or doubly ionized species, depending upon the spectral shape of the ionizing radiation and the ratio of ionizing flux to gas density. One expects that if the flux of ionizing photons is comparable to the flux of particles through the shock, the predicted spectrum will be strongly affected.

There are many B stars close to the Vela supernova remnant, but they are mostly of type B2 and later. Therefore, we assume that ζ Pup and γ Vel dominate the ionizing radiation and add radiation with a spectrum of a 40,000 K, log $g = 4.0$ Kurucz (1979) model. The dilution of this radiation depends on the distance between the star and the shock, but we can derive an upper limit from the great observed strength of [O II] relative to [O III]. The requirement of high O^+/O^{++} throughout the preshock gas requires a dilution factor below 10^{-17} for a preshock density of 2 cm^{-3}, or a distance of around 60 pc. The distance between the observed shock and γ Vel, which is probably a member of the Vela Association, is about 35 pc in the plane of the sky (assuming 500 pc from the Sun), so the true distance is unlikely to be much smaller than 60 pc. A dilution factor an order of magnitude smaller still ionizes the preshock gas, but a dilution factor smaller than that leaves the preshock gas neutral. The models require an ionized preshock medium, but we cannot discriminate between preshock ionization caused by Gum nebula stars and preshock ionization which occurred as the shock slowed from higher velocity. Such fossil ionization was inferred for the low-velocity portion of the Spur filament in the Cygnus Loop (RHCBFG). Thus we take a dilution factor of 10^{-18}, but only the upper limit of 10^{-17} is a well-established constraint.

Finally, the angle between the line of sight and the shock direction is not really a model parameter, but it does enter any comparison of emission or absorption lines with the models. All the column densities and surface brightness scale as $1/\cos(\theta)$, while the velocity shifts scale as $\cos(\theta)$. The only exceptions are the surface brightnesses of the resonance lines N V $\lambda1240$, Si IV $\lambda1400$, and C IV $\lambda1550$ (as well as C II $\lambda1335$ and Mg II $\lambda2800$ which we do not detect). These lines can have optical depths approaching unity along the flow direction, so that if $\cos(\theta)$ is small they become optically thick, and photons scatter out of the line of sight.

Under the above assumptions, we have computed some new shock models with the code described in Raymond (1979) and updated atomic rates summarized in Cox & Raymond (1985). The models are similar to those given in RHCBFG except for lower densities and different ratios of magnetic field to density. The shock velocities are chosen to match the highest observed ionization states, and we plot the ratios of emission-line intensities to Hβ as a function of swept-up column density (Fig. 3) and the total accumulated column densities of the observed ions as a function of N_H (Fig. 4).

3.2. *Absorption-Line Gas*

To interpret the absorption line measurements, we must first find v_s and the angle between the shock direction and the line of sight. The high-velocity component of C IV spans a range of 90–140 km s^{-1} away from the rest velocity of gas in that direction (-4 km s^{-1}; JWS). Steady flow models of $100 \le v_s$ to 160 km s^{-1} shocks show the C IV absorption centered at about 20 km s^{-1} less than the shock velocity, with a width of about 15 km s^{-1}. The low ionization lines should form at $0.98 \times v_s$, and they should be no more than 10 km s^{-1} wide. If we take the middle of the observed absorption line to be that given by the model, the angle between the shock direction and the line-of-sight is given by 125 km s^{-1} = $(v_s - 20)/\cos(\theta)$. The models predict a ratio of N V to C IV column densities of 0.15, 0.20, and 0.60 for 140, 150, and 160 km s^{-1} shocks, respectively. Thus the upper limit on the N V column density and the observed C IV column density place an upper limit of about 160 km s^{-1} on v_s, and the observed velocity displacement gives a lower limit of about 140 km s^{-1}. Thus we find $v_s = 150 \pm 10$

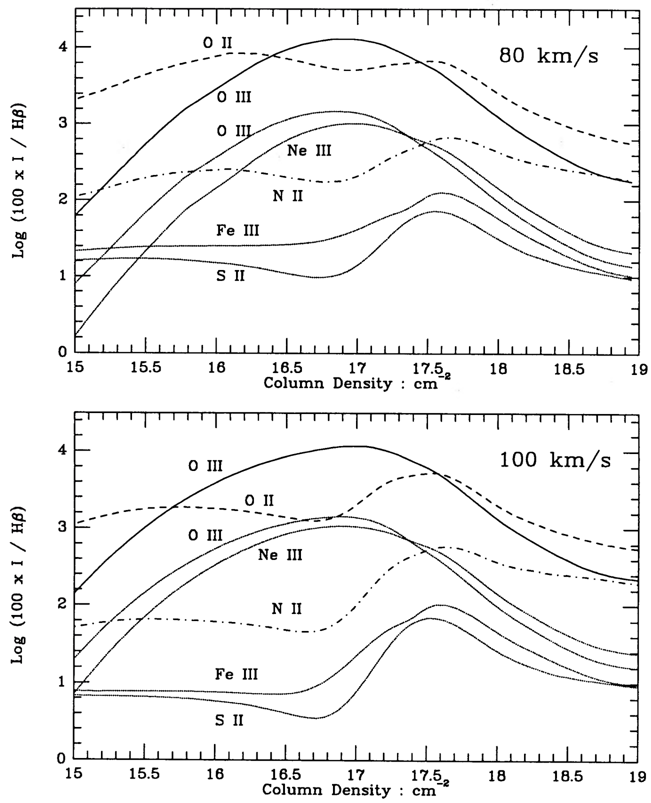

FIG. 3.—Emission-line intensities relative to $H\beta = 100$ as a function of total swept-up column density.

km s^{-1}. This velocity implies that the shock is nearly face-on, cos (θ) $\geq$ 0.85.

The models predict log ($N_{\mathrm{C\,IV}}$) = 13.42, and 13.20 along the flow direction for 140 and 160 km s^{-1} shocks. Thus both shock velocities give C IV column densities about 60% the observed value. There are several possible explanations for this discrepancy. It is larger than the uncertainty in the measured column density, but measurement error might account for half the problem. Uncertainties in the ionization and recombination rates of C IV are likewise expected to be around 30% (e.g.,

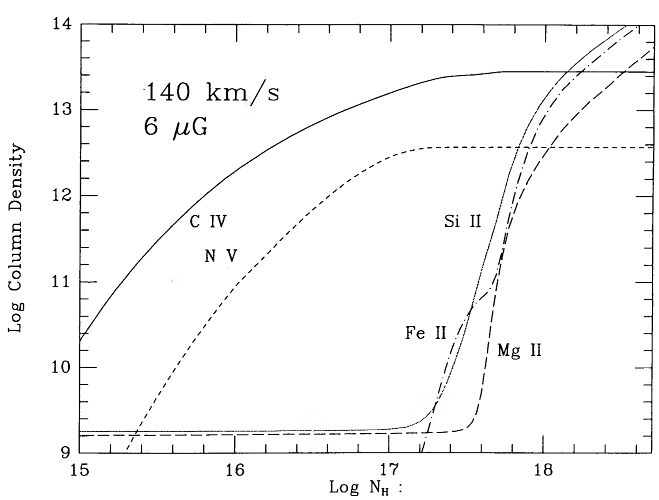

FIG. 4.—Column densities of observed ions as a function of swept-up hydrogen column density behind a 140 km s^{-1} shock.

RHCBFG). Thus, it is possible that a combination of model uncertainty and measurement uncertainty explains the discrepancy, though neither alone is adequate. The radiation field of the Gum nebula could in principle maintain the carbon ionization as C IV when it would otherwise have recombined to C III, but the strong [O II] relative to [O III] discussed below argues against this hypothesis.

There are two interesting astrophysical explanations for the strong C IV absorption. The more speculative is related to cosmic rays. The upper limit on shock velocity, and consequent lower limit on cos (θ), rely on an implicit assumption that the upper limit in T_s (which we derived from the lack of N V absorption) can be directly translated to a limit on v_s. This is true for an adiabatic shock, but if a large fraction of the shock energy goes into cosmic-ray acceleration, the true shock velocity is higher than that estimated from T_s. Estimates of the fraction of shock energy channeled into nonthermal particles generally range between 10% and 50% (e.g., Blandford & Eichler 1987; Boulares & Cox 1989). If half the shock energy goes into cosmic rays, the upper limit on T_s implies an upper limit on v_s near 200 km s^{-1} and a lower limit on cos (θ) near 0.6. The 1/cos (θ) enhancement of the C IV column density would then bring it into agreement with the observed value. This would not naturally explain the 50 km s^{-1} line width, however.

The second explanation for the high column density is thermally unstable cooling. Theoretical calculations show radiative shock waves faster than about 150 km s^{-1} to be violently unstable, with substantial oscillations in the shock velocity itself and formation of secondary shocks (e.g., Chevalier & Imamura 1982; Innes, Giddings, & Falle 1987). Such an instability is already suggested by the line widths. In a time-steady, plane-parallel flow, the C IV absorption should be about 20 km s^{-1} broad, and the Mg II and Si II lines should be no more than 10 km s^{-1} wide (including thermal broadening). The observed 50 km s^{-1} widths of the latter two ions require some sort of turbulence on a scale smaller than the cooling length (10^{17} cm/n_0; Hartigan, Raymond, & Hartmann 1987). Either thermal instability or small-scale, high-contrast density fluctuations in the preshock gas could broaden the lines. An argument for the instability explanation is the size of the discrepancy between observed and predicted column densities. The predicted thermal instability is violent because the gas cools so fast that it drops out of pressure equilibrium. The cooling proceeds nearly at constant density. This tends to decrease the predicted column densities in the cooling zone by a factor of 3/5 because only the internal energy, $3/2kT$, must be radiated away, as opposed to the enthalpy per particle $5/2\ kT$ at constant pressure. On the other hand, for a fixed flow rate through the shock, a lower density increases the column densities because the cooling time varies as $1/n_e$. If the gas drops out of pressure equilibrium as it cools from the shock temperature of 3×10^5 K, its pressure in the C IV zone is halved, and the C IV column density doubled. Combining the 3/5 decrease with the factor of two increase, one can naturally explain the factor of 1.6 discrepancy.

The model predictions for low stages of ionization depend not only on the assumed column density of swept-up gas, but also on the magnetic field. The magnetic field can stop the compression of the cooling gas and extend the thickness of the region required for recombination. Taking $v_s = 140$ km s^{-1}, $n_0 = 1.0$ cm^{-3}, $B_0 = 6\ \mu$G (to match the low density in the recombination zone discussed below), and cosmic abundances, we predict ion column densities as a function of hydrogen column shown in Figure 4. The observed column densities of Mg II, Si II, and Fe II require column densities log $N_H = 17.9$, 18.0, and ≤ 17.7, respectively. The C II* column density predicted by this model is 10^{14} cm^{-2}, which suggests that the density is even smaller than that predicted by the model, requiring a smaller value of n_0 or a larger B_0. This conclusion also requires faith in the relative abundances of C, Mg, and Si being the same as the cosmic values, however, which may not be fulfilled due to differential grain evaporation. If we could measure the column density of C II in the ground state, we could measure the density reliably, but the ground-state absorption line is saturated over the whole velocity range.

Finally, the C III] intensity derived from SWP 38718 can be probably ascribed to the same shock wave as seen in absorption, because the aperture was centered only 12″ away from the star. If the shock velocity is 150 km s^{-1} and cos (θ) is close to one, the preshock density must be about 2.0, so that the ram pressure $\rho_0 v_s^2$ is 9×10^{-10} dyn cm^{-2}. Wallerstein & Balick (1990) found $n_e \leq 70$ cm^{-3} from the [S II] doublet ratio, implying a thermal pressure $(n_e + n_i)kT \leq 2 \times 10^{-10}$ at 10^4 K. Kahn et al. (1985) derived the thermal pressure of the X-ray–emitting gas in the Vela SNR. They derived emission measures and temperatures for a dozen regions, and assuming a path length equal to the SNR diameter, they found a thermal pressure of 5×10^{-11} dyn cm^{-2}. The assumption of the maximum possible path length makes this pressure a lower limit, and the real value is likely to be twice as high, but it is very unlikely to be an order of magnitude larger. Thus we find that here, as in the Cygnus Loop (RHCBFG) the ram pressure of a cloud shock is several times larger than the thermal pressures in either the optically bright 10^4 K or the 10^6 K X-ray–emitting gas. In the case of this Vela SNR shock we have had to assume that cos (θ) is the same in front of HD 72088 and 12″ away, so the pressure discrepancy is not as securely established.

The discrepancy between ram pressure and the thermal pressure in the recombination zone might be attributed to the large pressure variations predicted by models of thermally unstable cooling behind shocks (Innes et al. 1987; Gaetz, Edgar, & Chevalier 1988), except that the inferred shock velocity of 150 km s^{-1} gives only marginal instability. Moreover, the upper limit on thermal pressure from the [S II] ratio applies to all the positions observed by WB, while one would except many positions to show high pressures behind thermally unstable shocks. The substantial nonthermal pressure component inferred here would not prevent the initial development of the thermal instabilities discussed above, but it would greatly soften the secondary shocks predicted by Innes et al. (1987).

3.3. *Emission-Line Region*

The region covered by SWP 39996 and LWP 19086 is the only one for which we have both long-wavelength and short-wavelength *IUE* spectra and optical spectra. Table 5E of WB gives the average of spectra covering about the same east-west position as the *IUE* aperture, and their spectra are 5″ S, 0″ N, and 5″ N of HD 72088 and the center of the *IUE* position. Thus, while the *IUE* positions include regions both north and south of those sampled by the optical spectra, the overlap is quite good. Given the lack of complete overlap, the uncertainty in absolute calibration, and the uncertainty in reddening, we do not attempt to merge the optical and UV spectra. Instead, Table 4 presents the UV line intensities relative to O III] $\lambda 1662 = 100$ and the optical intensities relative to Hβ = 100.

While the ratio of UV to optical lines are substantially affected by reddening, the relative intensities within the UV range or within the optical range are less sensitive, and the reddening of the Vela remnant is no more than $E(B-V) = 0.1$ (WB). Table 4 includes the relative intensities corrected for a reddening $E(B-V) = 0.1$ using the Seaton (1979) reddening curve. The uncertainties in the optical line ratios are probably similar to the UV uncertainties. The observed Hα-to-Hβ ratio is 20% below the recombination value, and this particular position was among the most deviant of the values given by WB, so we consider it a "2 σ" error.

By comparing the optical spectra of regions like this to the models given by RHCBFG, Wallerstein & Balick estimated a

TABLE 4

RELATIVE UV AND OPTICAL FLUXES

Ion	λ	Observed	Dereddened	80 km s^{-1}	90 km s^{-1}	100 km s^{-1}
N V	1240	≤16	≤17	...	...	2
O IV], Si IV	1400	58	61	140[a]	160[a]	170[a]
N IV]	1486	26	27	6	12	20
C IV	1550	92	94	120[a]	310[a]	580[a]
He II	1640	35	35	12	27	47
O III]	1662	100	100	100	100	100
N III]	1750	22	24	38	37	37
Si III]	1890	79	88	160	130	100
C III]	1909	210	239	370	360	360
C II]	2325	140	164	150	140	140
[Ne IV]	2420	≤20	≤20	1	5	14
[O II]	3727	5400	5900	5700	4900	4600
[Ne III]	3968	480	510	380	380	350
[S II]	4068	51	53	66	61	59
[O III]	4363	170	170	270	260	260
[Fe III]	4658	71	71	104	93	83
He II	4686	21	21	7	49	84
Hβ	4861	100	100	100	100	100
[O III]	5007	2800	2800	3200	3200	3200
Hα	6563	240	220	332	326	326
[N II]	6584	700	630	670	630	600

[a] Resonance scattering will reduce lines of C IV and Si IV are from the model values.

shock velocity of 80–100 km s^{-1}. Table 4 shows 80, 90, and 100 km s^{-1} models truncated at column densities of 4.0, 3.8, and 3.4×10^{17} cm^{-2}, respectively, all assuming 3 μG preshock magnetic fields. These column densities were chosen from Figure 3 to match the ratios of [O II] and [O III] to Hβ. The 80 km s^{-1} model matches the [O II] and [O III] lines best, while the higher velocities are better for the high-excitation He II and N IV] lines The C IV lines would help to determine the velocity more accurately, but they are affected by resonant scattering both in the emitting gas and in the intervening interstellar medium, so the model predictions are upper limits. We cannot separate the preshock density from cos (θ) with the available data, but if we assume $n_0 = 2$ as derived from the surface brightness close to HD 72088, then cos $(\theta) = 0.19$ to match the C III] surface brightness. The cutoff column densities are lower than those derived by WB because we have assumed a relatively weaker magnetic field. (Again, we have little direct evidence as to which is preferable.) WB obtained an upper limit to the density in the recombination zone from the [S II] lines $n_e \leq 70$ cm^{-3}. If $n_0 = 2$ cm^{-3}, this requires $B_0 \geq 3$ μG. On the other hand, if we assume the ram pressures of the emission-line cloud and the absorption-line shock to be equal, $n_0 = 4$ cm^{-3}, and $B_0 \geq 10$ μG. This field would require a cutoff column density near that obtained by WB.

Finally, we consider the elemental abundances. The C III]-to-O III] intensity ratio suggests a 40% depletion of carbon, while the C II]-to-O III] ratio suggests no depletion. This may be consistent with the Seab & Shull (1983) models which show carbon liberated from graphite grains largely by grain-grain collisions as the gas cools and compresses well behind the shock. However, the conclusion must be considered tentative because it is based on so few observed lines, and because SWP 39986 shows a C III]-to-O III] ratio in close agreement with the undepleted model. Similarly, the Si III] line suggests a silicon depletion of about 40% in SWP 39996, but no depletion in SWP 39986. In the optical, the [Fe III] line suggests a smaller depletion, in keeping with WB's comments that the optical spectrum agrees better with the RHCBFG models than do the optical spectra of RHCBFG. Dopita, Mathewson, & Ford (1977) derived abundances of 8.25, 7.6, and 6.6 for O, N, and S, respectively, from optical spectra of very low excitation filaments in the Vela supernova remnant. They used the shock models of Dopita (1977). Such low abundances make it impossible to match the spectrum given by WB. It is possible to reach a large enough O III-to-Hβ ratio, because hydrogen cannot cool the gas effectively at the higher temperatures, but models with the lower abundances fail to match the O II strength by a factor of 2. We believe that the greater sensitivity of slower shocks to preshock ionization conditions, together with the limited wavelength coverage of their spectra and the uncertainties in the earlier generation of shock models, caused Dopita et al. to underestimate the abundances. Raymond et al. (1981) analyzed *IUE* spectra of one filament near the center of the Vela SNR. That position showed a C III]-to-O III] ratio intermediate between the values of Table 2, and the spectrum was adequately matched with the cosmic C-to-O and O-to-H ratios.

4. SUMMARY

Ultraviolet spectra of nebulosity near HD 72088 confirm the shock velocity (80–100 km s^{-1}) and shock incompleteness determined by Wallerstein and Balick. The shock seen in absorption in front of the star is faster and nearly face-on, while the bright emission-line cloud is close to edge-on. There is some evidence for depletion of carbon and silicon, and for a smaller depletion of iron. Absorption lines in the spectrum of the star imply a higher velocity shock, and they suggest thermally unstable cooling to account for the line widths and excess C IV absorption. Depletion of carbon would exacerbate the difficulty in producing a large enough C IV column density, so the faster shock may destroy carbon-bearing grains by sputtering in the higher temperature part of the flow. The modest C II* column density effectively places an upper limit on the density of the recombination region. If the preshock density is correctly given by the C III surface brightness 12″ away from the star, then in this portion of the Vela supernova remnant, as in the Cygnus Loop filament observed by RHCBFG, the thermal pressure of the recombining gas is far smaller than the pressure of the shock. This suggests that a strong transverse magnetic field exists in the preshock gas or that cosmic-ray acceleration takes a substantial portion of the energy dissipated by the shock.

We wish to thank the *IUE* staff and D. Zucker for help in the acquisition and reduction of the data. This work was supported by NASA grant NAS5-87 to the Smithsonian Astrophysical Observatory. The work of G. W. and B. B. was supported by NASA grant NAG5-1443.

REFERENCES

Allen, C. W. 1973, Astrophysical Quantities (3d ed.; London: Athlone)
Benvenuti, P., Dopita, M., & D'Odorico, S. 1989, ApJ, 238, 601
Blandford, R., & Eichler, D. 1987, Phys. Rept., 154, 1
Boggess, A., et al. 1978, Nature, 275, 372
Boulares, A., & Cox, D. P. 1989, ApJ, 333, 198
Chevalier, R. A., & Imamura, J. N. 1982, ApJ, 261, 543
Crenshaw, D. M., Bruegman, O. W., & Norman, D. J. 1990, PASP, 102, 463
Cox, D. P. 1972, ApJ, 178, 159
Cox, D. P., & Raymond, J. C. 1985, ApJ, 298, 651
Dopita, M. A. 1977, ApJS, 33, 437
Dopita, M. A., Binnette, L., & Tuohy, I. R. 1984, ApJ, 282, 142
Dopita, M. A., Mathewson, D. S., & Ford, V. L. 1977, ApJ, 214, 179
Draine, B. T., & Salpeter, E. E. 1979, ApJ, 231, 438
Fesen, R. A., Blair, W. P., & Kirshner, R. P. 1982, ApJ, 262, 171
Fesen, R. A., Wu, C.-C., Leventhal, M., & Hamilton, A. J. G. 1988, ApJ, 327, 164
Gaetz, T. A., Edgar, R. J., & Chevalier, R. A. 1988, ApJ, 329, 927
Hartigan, P., Raymond, J., & Hartmann, L. 1987, ApJ, 316, 323
Innes, D. E., Giddings, J. E., & Falle, S. A. E. G. 1987, MNRAS, 226, 67
Jenkins, E. B., & Shaya, E. J. 1979, ApJ, 231, 55
Jenkins, E. B., Silk, J., & Wallerstein, G. 1976, ApJS, 32, 681
Jenkins, E. B., Wallerstein, G., & Silk, J. 1984, ApJ, 278, 649 (JWS)
Kahn, S. M., Gorenstein, P., Harnden, F. R., Jr., & Seward, F. D. 1985, ApJ, 299, 821
Kurucz, R. L. 1979, ApJS, 40, 1
Luo, D., Pradhan, A. K., & Shull, J. M. 1988, ApJ, 335, 498
McKee, C. F., & Cowie, L. L. 1979, ApJ, 195, 715
McKee, C. F., & Hollenbach, D. J. 1980, ARA&A, 18, 219
Raymond, J. C. 1979, ApJS, 39, 1
Raymond, J. C., Black, J. H., Dupree, A. K., Hartmann, L., & Wolff, R. S. 1980, ApJ, 238, 881
———. 1981, ApJ, 246, 100
Raymond, J. C., Hester, J. J., Cox, D. P., Blair, W. P., Fesen, R. A., & Gull, T. R. 1988, ApJ, 324, 869 (RHCBFG)
Seab, G. C., & Shull, J. M. 1983, ApJ, 275, 652
Seaton, M. J. 1979, MNRAS, 187, 73P
Shull, J. M., & McKee, C. F. 1979, ApJ, 227, 131
Wallerstein, G., & Balick, B. 1990, MNRAS, 245, 701 (WB)